How entanglements determine the morphology of semicrystalline polymers

Zefan Wang
Martin-Luther Universität Halle-Wittenberg https://orcid.org/0000-0003-1137-5433
Mareen Schäfer
Martin-Luther Universität Halle-Wittenberg
Albrecht Petzold
Martin Luther University Halle-Wittenberg https://orcid.org/0000-0002-2920-7019
Kay Saalwächter
Martin-Luther-Universität Halle-Wittenberg https://orcid.org/0000-0002-6246-4770
Thomas Thurn-Albrecht (thurn-albrecht@physik.uni-halle.de)
Martin-Luther Universität Halle-Wittenberg https://orcid.org/0000-0002-7618-0218

Article

Keywords:

Posted Date: August 19th, 2022

DOI: https://doi.org/10.21203/rs.3.rs-1839187/v1

How entanglements determine the morphology of semicrystalline polymers

Zefan Wang,[†] Mareen Schäfer,[‡] Albrecht Petzold,[†] Kay Saalwächter,[‡] and Thomas Thurn-Albrecht[*,†]

†*Institute of Physics, Experimental polymer physics group, Martin Luther University, Halle-Wittenberg, 06120, Halle, Germany*

‡*Institut für Physik – NMR, Martin-Luther-Universität Halle-Wittenberg, 06099 Halle (Saale), Germany*

E-mail: thurn-albrecht@physik.uni-halle.de

Abstract

Crystallization of polymers from entangled melts generally leads to the formation of semicrystalline materials with a nanoscopic lamellar morphology. Controlling this structure is key to the rational design, application and possible re-use of thermoplastic materials, but there is no consensus yet on the factors that control the thickness of the amorphous layers. We elucidate the effect of entanglements on the morphology in a series of model blends of high-molecular-weight polymers with unentangled oligomers leading to a reduced entanglement density as characterized by rheological measurements in the melt. Small-angle X-ray scattering experiments after isothermal crystallization reveal a reduced thickness of the amorphous layers, while the crystal thickness remains largely unaffected. A simple yet quantitative model without adjustable parameter is suggested, according to which the measured thickness of the amorphous layers adjusts itself in such a way that the entanglement concentration reaches a specific maximum value.

Introduction

Due to their favorable mechanical properties and their simple processability, crystallizable polymers make up the majority of thermoplastics and are used in a broad field of different applications. In particular the current trend towards better-recyclable and possibly chemically less diverse materials relies on understanding and controlling their mechanical properties. These are governed by their semicrystalline morphology made of nm-thin lamellar crystals separated by disordered amorphous layers.[1,2] The mechanical properties at small deformations are determined by the crystalline scaffold in the material leading to a high modulus that increases with crystallinity, whereas the existence of entanglements and tie molecules in the amorphous phase is responsible for strain hardening at large deformations and for toughness.[2–5] The factors governing the crystal thickness have been extensively studied,[2,6–11] but the corresponding yet no less important question for the amorphous regions has obtained much less attention. While it has been suggested that the entanglements in the amorphous regions limit the crystallinity of polymers undergoing crystallization from the melt,[12,13] experimental evidence is inconclusive and the effects of the entanglements on the semicrystalline morphology are not well understood.

Addressing this question faces fundamental difficulties. First and foremost, the concentration of entanglement strands, or equivalently, the molecular weight (MW) between entanglements, is an inherent property of a given polymeric material and cannot be varied in a simple way. While unentangled high-MW melts have been prepared by melting of unentangled crystalline material, which was either prepared by direct crystallization during synthesis or from dilute solution or from the hexagonal high-pressure phase of polyethylene (PE),[14,15] such melts are in a heterogeneous non-equilibrium state that is unstable, as chain diffusion typically reestablishes the entangled state relatively quickly.[15,16] Studies on non-equilibrium disentangled PE melts made in this way suggested increased crystal growth rates and a lower nucleation density but no effect on the long period seen in small-angle X-ray scattering (SAXS).[14,17] There have been attempts to vary the concentration of entanglement

strands via dilution with low-MW solvents, leading to changes in crystal thickness for some solvents, but without a quantitative account of entanglement density.[18]

General caveats of such studies are the solvent-related melting point depression, and that the solvent concentration increases during crystallization, which means that the driving force for crystallization is not constant during the process. A recent study along these lines did indicate lower amorphous thicknesses in systems crystallizing from solutions with decreasing concentrations,[19] but the SAXS data could not be analyzed quantitatively due to inhomogeneities due to the remaining solvent not participating in the crystallization, thus providing only indirect evidence relying on DSC crystallinity. Furthermore, the reduced entanglement strand concentrations were only estimated by a scaling law, but the exponent used did not conform to the textbook value.[20] Turning to theory, Luo and Sommer studied the effect of entanglements in simulations.[21,22] Here, the entanglement length was either varied indirectly due to the temperature-dependent conformation of the polymers or by crystallization from solution, where short chains with otherwise identical properties were used as a solvent. While the amorphous regions were not explicitly considered, an interesting increase of the crystal thickness with decreasing degree of entanglement was found, suggesting that the crystal thickness might in fact be governed by the entanglements in the melt prior to crystallization.

Here we present an experimental approach that avoids all of the above-mentioned difficulties and allows us to directly study the effect of entanglements on the semicrystalline morphology in a quantitative way and thus to establish a predictive model. We prepared a series of melt samples with reduced concentration of entanglement strands in equilibrium by mixing a melt of a high-MW polymer with chemically identical unentangled oligomers (cf. Table 1). The resulting concentration of entanglement strands was determined by rheological analysis. Importantly, polymer and oligomers cocrystallize without phase separation for larger supercooling, allowing a direct quantitative in-situ analysis of the semicrystalline morphology by SAXS as a function of the entanglement concentration in the melt. As a model

polymer we used polycaprolactone (PCL), for which we could recently show by advanced NMR techniques that entanglements are fully retained during crystallizaton from the melt, thus increasing the entanglement density in the amorphous phase upon crystallization.[23]

Results

Reduced entanglement concentration in polymer/oligomer blends. Shear rheology was used to characterize all samples in the melt state via frequency sweeps at 90, 70, 50 °C. Master curves for the storage and loss moduli (G' and G'', resp.) with a reference temperature of 50 °C were constructed by time-temperature superposition,[24] see Figure 1 (for original data, see the Supplementary Information, Figure S1). Note that experiments below the melting temperature are still possible due to slow crystallization. Terminal flow is always apparent on the low-frequency side, while for all samples except the one with the lowest polymer concentration, G' approaches a rubber-elastic plateau with modulus G_0 on the high-frequency side. Obviously, the measurements show qualitatively the results expected for a semidilute solution, namely a decrease of G_0 and τ_d with decreasing polymer fraction ϕ.

Due to the limited frequency range of the instrument and the limited accessible temperature range due to crystallization at low temperatures, it was not possible to read off G_0 in the center of the plateau where G'' reaches a minimum, as it is usually done. Instead, for a quantitative determination G_0 was determined by integration of G'' for $\phi = 1$ resulting in a value of 1.26 MPa for G_0, cf. Fig. S2:[25–28]

$$G_0\left(\phi = 1\right) = \frac{2}{\pi} \cdot \int_{-\infty}^{+\infty} G''\left(\omega, \phi = 1\right) dln\omega \tag{1}$$

While this method cannot be applied to the diluted samples, since the relaxation time spectrum revealed on the high-frequency side of G'' changes, we can assume that there is a constant factor between the plateau modulus G_0 and the value of G'_{ω_d} at the crossover

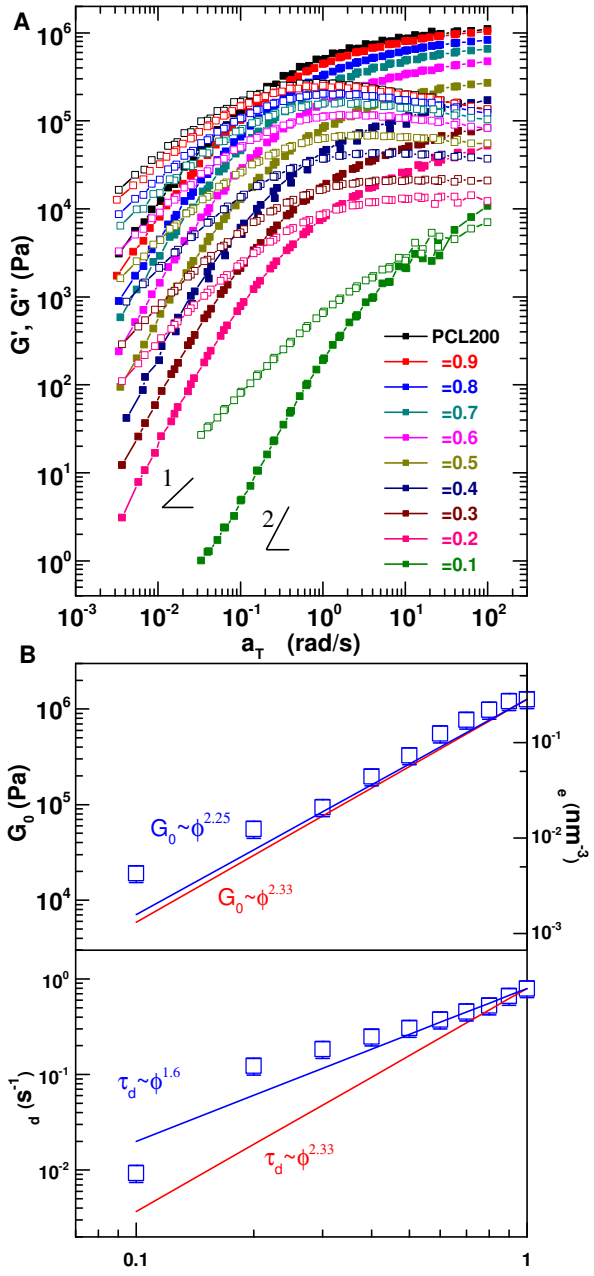

Figure 1: **Rheological characterisation of polymer/oligomer blends in the melt state.** A) Master curves of storage modulus G' (closed symbols) and loss modulus G'' (open symbols) of blends with different polymer fraction ϕ referenced to 50 °C, with indicated power laws for terminal flow. B) Plateau modulus G_0 (lhs scale) together with concentration of entanglement strands ν_e (rhs scale) and terminal relaxation time τ_d as a function of ϕ. Blue and red lines show the expected power laws for good and θ-solvents, respectively.

frequency ω_d of the moduli. We thus estimate $G_0(\phi)$ as

$$G_0(\phi) = \frac{G_{\omega_d}(\phi)}{G_{\omega_d}(\phi = 1)} \cdot G_0(\phi = 1). \tag{2}$$

Based on the theory of rubber elasticity, the plateau modulus is related to the entanglement strand concentration ν_e as follows.[20,24,29]

$$G_0(\phi) = \nu_e(\phi) k_B T = \frac{\rho RT}{M_e(\phi)} \tag{3}$$

The resulting values of $\nu_e(\phi)$ are shown together with $G_0(\phi)$ in Figure 1B. For the pure polymer $M_e = (\rho_m RT)/G_0 = 2.346$ kg/mol . Here the density in the melt state $\rho = 1.11$ kg/m^3 was estimated from the tabulated densities of semi-crystalline PCL and the crystal density, $\rho_{sc} = 1.145$ kg/m^3; $\rho_c = 1.20$ kg/m^3 respectively,[30] based on $\rho_{sc} = \rho(1 - X_c) + \rho_c X_c$ with a volume crystallinity $Xc = 40\%$, obtained from SAXS.

To ensure consistency, we compare the measured values of G_0 and τ_d (taken as the inverse of the modulus crossover frequency) with the known scaling laws for semidilute solutions. Neglecting chain-end effects we would expect the oligomers to behave as a good, even athermal, solvent as they are chemically identical to the polymer. The plateau moduli in good and θ solvents scale as $G_0 \sim \phi^{2.25}$ and $G_0 \sim \phi^{2.33}$, respectively[20,29] and our data follow these rather similar predictions very well (cf. Figure 1B). The solvent quality has a stronger effect on the scaling law for the disentanglemant time τ_d,[20] where $\tau_d \sim \phi^{1.6}$ and $\tau_d \sim \phi^{2.3}$ for the different solvents, respectively. As shown in Figure 1C, the data are much better described by the prediction for the good-solvent case, as expected for our chemically similar oligomers. Only the 10% solution deviates significantly, as it is not fully entangled (see Supplementary Text 1).

No phase separation on crystallization. The second important feature of our model system is that that both components crystallize in a single phase. As the polymer has a

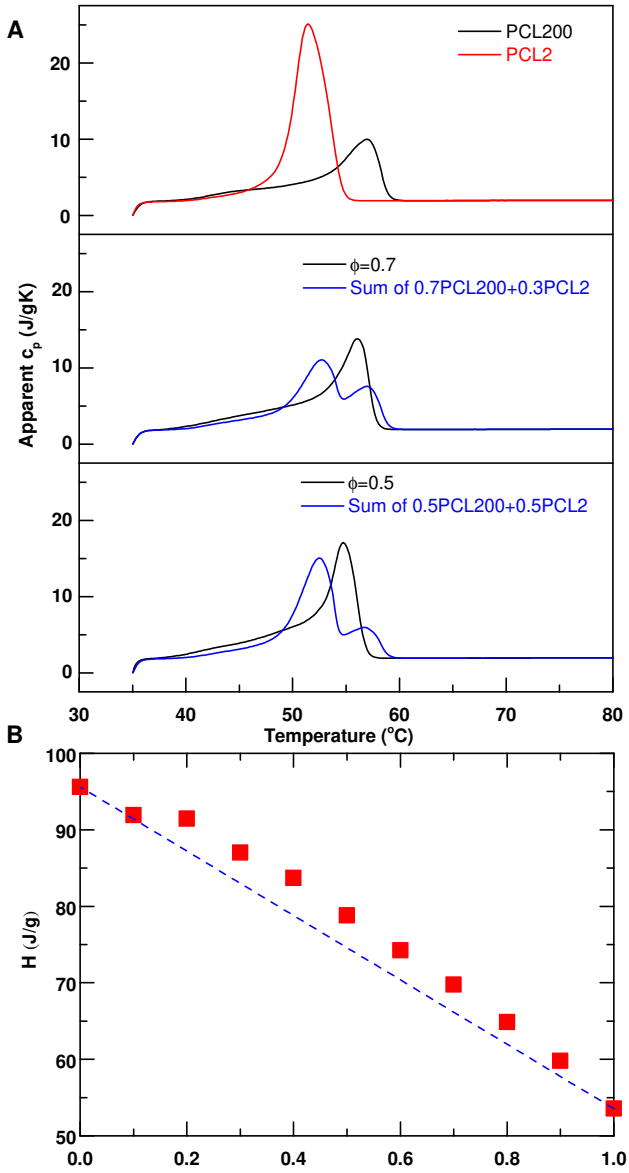

Figure 2: **Calorimetric characterisation of polymer/oligomer blends.** A) DSC heating curves for PCL200 and PCL2 after isothermal crystallization at 35 °C (top) and comparison of heating curves of blends (black) with $\phi = 0.7$ (middle) and $\phi = 0.5$ (bottom) with the weighted sum of the component curves (blue). B) Melting enthalpy vs. composition ϕ for all blends. The blue dashed line shows the weighted sum of the melting enthalpies.

higher melting temperature than the oligomer, it may be expected that crystallization at low supercooling will lead to a preferred or even exclusive crystallization of the polymer, resulting in a separation. However, we can prove that such effects can be suppressed by crystallization at low temperatures, i.e. high supercooling.

Figure 2A shows heating curves measured by differential scanning calorimetry (DSC) of the pure components and two exemplary blends with ϕ =0.7 and ϕ = 0.5 after isothermal crystallization at the chosen crystallization temperature, T_c =35 °C (see Figure S3 for the full data set for all compositions). As mentioned above, the polymer shows a higher melting temperature (peak temperature 58.9 °C) than the oligomer (peak temperature 54.6 °C). Generally, the integral over the melting range gives the enthalpy of melting and is proportional to the crystallinity of the sample, indicating here the higher crystallinity of the oligomer in comparison to the polymer. We clearly see that the melting signal of the blends does not correspond to a superposition of the signals of the components, as it would be the case for a separate crystallization of the components. Instead, melting occurs at an intermediate temperature, indicating a composite semicrystalline structure resulting from cocrystallization. This conclusion is confirmed by the enthalpies of melting shown in Figure 2B, which for the blends are generally larger than the sum of the enthalpies of the components weighted according to weight fractions. The DSC results together with the results from the rheological measurements confirm that our samples constitute a well-suited model system to study the effects of the entanglement concentration on the morphology of semicrystalline polymers in a quantitative way.

Entanglement-controlled semicrystalline morphology. SAXS measurements combined with a recently developed refined method of analysis based the linear stack model (Figure 3A) allow us to determine the mean thickness of the crystalline and amorphous regions as well as their distribution widths as described in the method section.[31–33] SAXS data for the pure polymer, oligomer and all blends measured at 35 °C after isothermal crys-

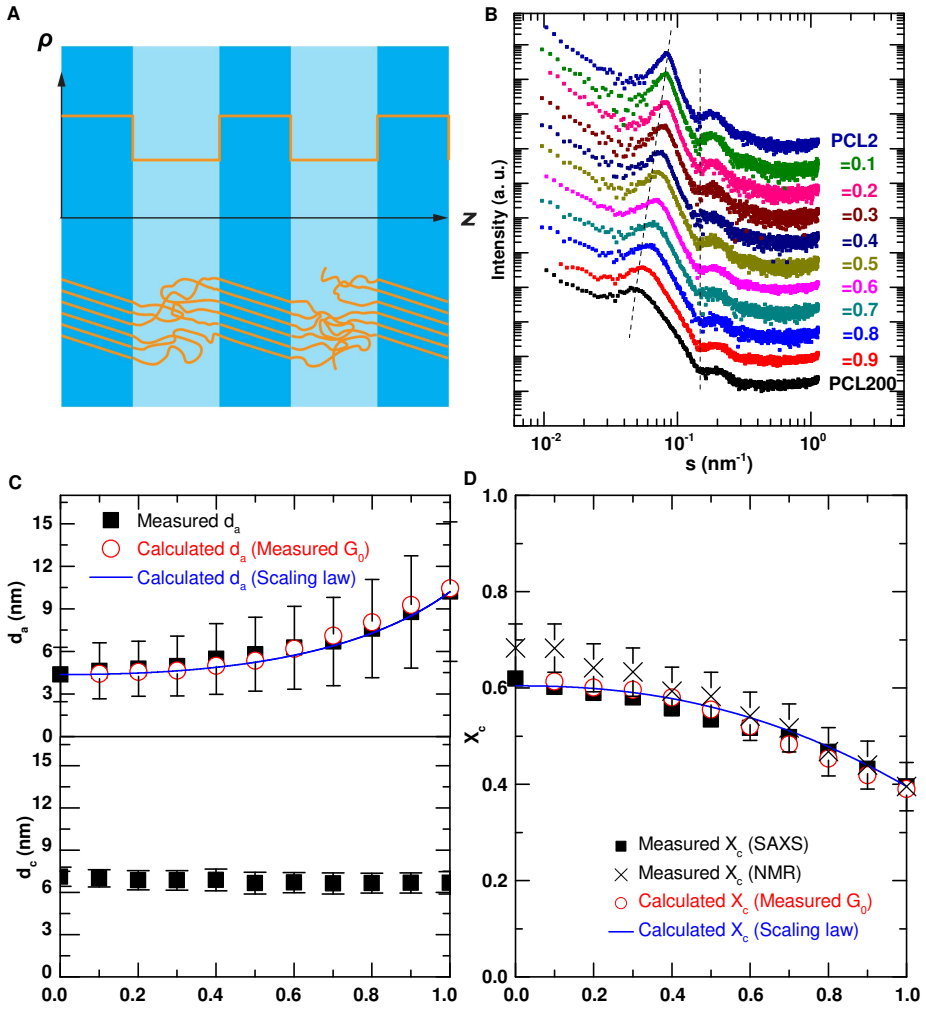

Figure 3: **Characterization of the semicrystalline morphology by SAXS and NMR**. A) Sketch of the semicrystalline morphology consisting of a stack of alternating crystalline and amorphous layers. B) SAXS intensity vs. scattering vector s of polymer/oligomer blends after isothermal crystallization at 35 °C, shifted vertically for clarity. C) Thickness of the derived crystalline and amorphous regions d_c and d_a (black filled squares) as a function of ϕ, with vertical bars indicating the respective distribution widths σ_c and σ_a. D) Crystallinity vs. ϕ as determined by SAXS and NMR. Open circles and solid lines in C, D are the predictions of our model, based upon measured values of the melt-state plateau modulus and on the scaling law for the entanglement concentration in good solvents ($\nu_e \sim G_0 \sim \phi^{2.25}$), respectively.

tallization are shown in Figure 3B. With decreasing polymer fraction, the peak caused by the decreasing long period shifts towards higher scattering vectors s. At the same time, the characteristic minimum at $s \approx 0.14\,\mathrm{nm}^{-1}$, which is caused by the minimum in the form factor of the crystalline lamellae remains at the same position. These observations already qualitatively indicate a decreasing thickness of the amorphous regions with decreasing polymer fraction.

The structural parameters resulting from the fully quantitative analysis of the SAXS data, namely the thickness of the crystalline and amorphous regions d_c, d_a and their distribution widths σ_c, σ_a are shown in Figure 3C as a function of the polymer fraction ϕ. The details of the quantitative analysis are described in the Supplementary Information, Supplementary Text 2 and Figures S4–S8. The similarity of the linear crystallinity $X_c = \frac{d_c}{d_c+d_a}$ from SAXS with the NMR crystallinity based on a decomposition of the ^{1}H FID-signal confirms the assignment of d_c and d_a and shows the applicability of the linear stack model. For the pure polymer, the morphology corresponds to previous observations.[32] The crystal thickness is smaller than the thickness of the amorphous regions with a much sharper distribution of the crystal thickness. With decreasing polymer fraction the crystal thickness remains unchanged while the thickness of the amorphous regions decreases by about a factor of 2. The distributions keep their characteristic differences and the long period $d_{ac} = d_c + d_a$ follows the changes in d_c and d_a. Obviously, the thickness of the amorphous regions is in fact determined by the concentration of entanglement strands, suggesting a composition-dependent minimal thickness of the amorphous regions, beyond which the entanglements cannot be compressed any further.

A quantitative model. To justify a simple yet quantitative prediction of d_a based on a maximum concentration of entanglement strands $\nu_{e,max}$, we already showed in a previous publication that for PCL, entanglements are retained during crystallization from the entangled melt.[34] In consequence, we should be able to determine $\nu_{e,max}$ from the structural

parameters of the pure polymer. Furthermore, we have to take into account that even for the oligomers ($\phi = 0$), which are unentangled, we observe amorphous regions in-between neighboring crystallites. For the model we make the most basic assumption that they consist of two partially ordered, constrained amorphous boundary layers with thickness $d_{a,b} = 2.2$ nm and that these boundary layers exist for all compositions and have always the same thickness, therefore $d_a(\phi) = d_{a,i}(\phi) + 2d_{a,b} = d_{a,i}(\phi) + d_a(\phi = 0)$. We assume that only the additional inner part with thickness $d_{a,i}$ contains the fully retained entanglements. If we further assume that the thickness of the inner amorphous regions $d_{a,i}$ after isothermal crystallization is given by the condition of a constant value of $\nu_{e,max}$, the following equation holds for all compositions ϕ:

$$\frac{d_{a,i}(\phi)}{d_c(\phi) + 2d_{a,b} + d_{a,i}(\phi)} = \frac{\nu_e(\phi)}{\nu_{e,max}} \tag{4}$$

Solving this equation for d_a gives:

$$d_a(\phi) = 2d_{a,b} + \left(\frac{\nu_{e,max}}{\nu_e(\phi)} - 1\right)^{-1} (d_c(\phi) + 2d_{a,b}) \tag{5}$$

Furthermore we can use:

$$\frac{\nu_{e,max}}{\nu_e(\phi)} = \frac{\nu_{e,max}}{\nu_e(\phi = 1)} \cdot \frac{\nu_e(\phi = 1)}{\nu_e(\phi)} = \frac{d_c(\phi = 1) + d_a(\phi = 1)}{d_{a,i}(\phi = 1)} \cdot \frac{G_0(\phi = 1)}{G_0(\phi)} \tag{6}$$

Eqs. 5 and 6 allow us to predict d_a (cf. Fig. 3C) as well as the linear crystallinity $X_c = \frac{d_c}{d_c + d_a}$ (cf. Fig. 3D) without any adjustable parameter. The very good agreement with the values measured by SAXS are a strong indication that the thickness of the amorphous regions is indeed determined by the assumed condition of a constant, maximum concentration of entanglement strands. From eq. (4) and our SAXS data, we derive $\nu_{e,max}/\nu_e(\Phi = 1) = 2.9$ as the relevant outcome of our analysis. Entanglements can obviously be compressed in the amorphous regions to quite an extent. The factor of 2.9 is close to our previous direct

NMR-based estimation of around 2,[23] which was obtained as an average over the whole amorphous layer, not just the inner part. Together with further previous results, where we showed that the crystal thickness in PCL directly after crystallization corresponds to the minimum thickness required for thermal stability,[32,33] we thus achieved here for the first time a full empirical understanding of the criteria that determine the structural parameters of the semicrystalline morphology during isothermal crystallization, including the important parameter crystallinity.

Discussion

The assumption of the boundary layer is based on the morphology of the pure oligomer and the observation that the structural parameters vary smoothly from the oligomer over the blends to the polymer. In comparison to previous experiments on oligomers, mostly performed on long alkanes or oligomers of PEO, the value of the oligomer crystallinity seems low. However, PE and PEO are known for their ability of fast reorganization based on chain diffusion through the crystals, which leads to a state of extended or integer-folded chains with high crystallinity. Non-integer folded states with lower crystallinity transform quickly into high-crystallinity states.[35] In the case of PCL such a process is absent or very slow.[32] Experiments on oligomers without intracrystalline chain diffusion are scarce, but our results are indeed consistent with previous observations for a series of precise oligomeric PCL.[36]

With regards to chain conformation, our oligomer with on average 20 monomers and an extended length of 17.2 nm is less than twice the 11.6 nm long period, ruling out a dominance of once-folded chains. On the other extreme, a fully extended conformation with a significant lamellar tilt angle, a common phenomenon,[37] is consistent with the observed structure. The true structure in-between these two limits is certainly governed by the polydispersity, which also limits the crystallinity of the oligomer. Generally, three-phase models are often used to describe the semicrystalline morphology, and they are typically necessary for the

interpretation of experimental data, for which the phases are identified based on different molecular mobility like in DSC or NMR. As is apparent from the comparison of our NMR-based component decomposition (Fig. S9), the entanglement-free boundary layer is larger than the NMR-based "rigid-amorphous fraction."

Our analysis also suggests a new explanation as to why the temperature range (and therefore thickness range) in which crystallization occurs is always lying well below the equilibrium melting temperature. PCL e.g. crystallizes only at temperatures below about 60 °C, corresponding to crystal thicknesses below about 10 nm, although thermodynamically the crystallization of thicker lamellae at higher temperatures should be feasible.[38] We hypothesize that the crystal thickness is limited by the length scale over which the crystallizing melt can be cleared of entanglements by compressing them into the amorphous regions. If the entanglement network was fixed, the tube diameter a would certainly be an upper limit for the crystal thickness plus the boundary layers. However, the entanglement network can locally rearrange and the entanglements can be compressed in the amorphous regions by the above-determined factor of 2.9. For PCL $a = \sqrt{N_e b^2} = 3,67$ nm, resulting in a value of $3.67 \text{ nm} \cdot 2.9 = 10.6$ nm for $d_c + 2d_{a,b}$, i.e. $d_c \approx 6.2$ nm, an estimate that fits very well to the SAXS-result for d_c, cf. Fig. 3. Here we used $N_e = \frac{M_e}{M} N_k$; the corresponding values are given in the Methods section. We note that these data and thus our model are fully consistent with the recent findings that the lamellar thickness and adjacent folding numbers are largely governed by the entanglement spacing and the contour length of an entangled segment.[39,40]

As a final point, it is important for the arguments made above that entanglements are not significantly dissolved during crystallization. While we could explicitly show that this is indeed the case for PCL,[23] we believe that this assumption is generally true for so-called crystal-fixed polymers, which have no or only very slow intracrystalline chain diffusion. Crystallization generally proceeds too fast to allow substantial resolution of entanglements at the growth front.[34] On the other hand, polymers with intracrystalline chain diffusion, so-called crystal-mobile polymers show crystal thickening during crystallization leading to

crystallinities well-above 50% while the thickness of the amorphous regions is of similar size as in case of crystal-fixed polymers[11,32]. A resolution of entanglements in these systems could arise from intracrystalline chain diffusion. The existence of such a process is obvious in the case of high-pressure crystallization of PE into the hexagonal mesophase leading to practically 100% crystalline material,[41] wheras in ambient crystallization, where it develops a semicrystalline morphology of relatively high crystallinity, there is only indirect evidence.[4] A direct quantitative determination of the entanglement density in the semicrystalline state for crystal-mobile polymers in combination with a detailed structural analysis would allow us to prove that also for crystal-mobile polymers, the thickness of the amorphous layers is determined by the maximum concentration of entanglement strands. This question is left for future work.

In summary, using a specifically designed experimental system we have demonstrated that a simple yet quantitative model, assuming a material-specific maximal entanglement concentration in the inner amorphous layer, can explain one of the most outstanding and so far little explored morphological features of semicrystalline polymers, i.e. the thickness of the amorphous layers and thus also the overall crystallinity. This finding is of high relevance with regards to understanding and controlling the mechanical properties, which are obviously determined by this scaffold structure. In our case, the modulus increases by nearly a factor of two in the range from $\phi = 1$ to $\phi = 0.5$ (see Figure S10), highlighting the potential of using high/low MW blends to control the mechanical properties of materials; an insight that might also be important for the recycling of thermoplastic materials.

Methods

Materials

Polycaprolactone polymer PCL200 and oligomer PCL2 were purchased from Scientific Polymer Product Inc., Ontario, New York (USA). Due to the low MW ($M \approx M_e$) the oligomer

Table 1: Properties of PCL polymer and oligomer samples. M_w and M_n are the weight-averaged and number-averaged MW as obained from the product data sheet. N, R_{max}, R_0 are the number averaged values of the degree of polymerization, extended chain length, and the end-to-end distance.

	M_w (kg/mol)	M_n (kg/mol)	N	R_{max} (nm)	R_0 (nm)
PCL200	200.7	188.1	1650	1424	34.0
PCL2	2.38	2.27	20	17.26	3.73

is unentangled. Basic sample characteristics are listed in Table 1. They were calculated as follows. The extended chain length is given by $R_{max} = N \cdot l$. Here $l = c/2 = 0.863$ nm, where c is unit cell parameter of PCL.[42] The end-to-end distance is given by $R_0 = 0.0783\sqrt{M}$ nm$\sqrt{\text{mol/g}}$.[43] From the data for PCL200 the Kuhn length b can be calculated, $b = \frac{R_0^2}{R_{Max}} = 0.81nm$ and the number of Kuhn segments as $N_k = \frac{R_{Max}^2}{R^2} = 1758$.[20]

Polymer/oligomer blends with polymer weight fractions ϕ from 10% to 90% were prepared from mixed solutions in chloroform with a concentration of 25mg/ml, which were stirred for 2 hours and subsequently dried in a fume hood for 4 days. To remove residual solvent the samples were additionally kept in vacuum for 24h. Before any experiments the samples were heated to 85 °C for 10 min to remove the thermal history.

Methods

Small-angle X-ray diffraction SAXS measurements were performed on a Kratky compact camera from Anton Paar GmbH, Graz equipped with an X-ray optics from AXO Dresden GmbH, a temperature-controlled sample holder and a 1D detector Mythen2 R 1K from Dectris. All samples were isothermally crystallized in the Kratky camera for 30 min after a quench from the melt state (10 min at 85 °C). The exposure time for each scattering curve was 30 min. Although the setup allows a measurement of the primary beam intensity and therefore nominally a determination of the absolute scattering intensity, there was a certain error in the scattering volume due to some air bubbles in the samples. The measured scattering curves were therefore multiplied by a correction factor such that the intensity at large

scattering vectors q due to the density fluctuations in the amorphous regions is on the same level for all measurements. This procedure brings the amplitudes of the interface distribution functions to comparable amplitudes, although they are not evaluated quantitatively.

The analysis of the SAXS data is based on the interface distribution function (IDF) $K''(z)$, originally introduced by Ruland.[44] Below we give a brief account of the method. The procedure for analysis has been described in detail in previous publications.[31,32,45] In the last reference we additionionally specifically discussed the method in comparison to the common direct analysis of the correlation function. In the SM we describe the data treatment including background subtractions, illustrate the different steps of the analysis and show the orginal data, cf. Fig. S4 - Fig. S8.

For a stack of alternating cystalline and amorphous regions with sharp interfaces between the two phases the interface distribution function K'' can be calculated from the SAXS intensity data (after background subtraction) as follows:

$$K''(z) = 16\pi^3 \int_0^\infty [\lim_{s\to\infty} I(s)s^4 - I(s)s^4] \cos(2\pi sz) ds, \tag{7}$$

where $s = \frac{2}{\lambda}\sin\theta$ is the scattering vector and $\lim_{s\to\infty} I(s)s^4$ the Porod constant P. The proportionality $I(s) \propto s^{-4}$ and the constraint $K''(0) = 0$ are consistency conditions for the assumptions of sharp interfaces and negligible contributions from lateral interfaces of the crystallites. On the other hand, K'' is related to the semicrystalline structure by

$$K''(z) = \frac{O_s \Delta\rho^2}{2}(h_a(z) + h_c(z) - 2h_{ac}(z) + h_{aca}(z) + ...) \tag{8}$$

Here the thickness distributions of the alternating crystalline (h_c) and amorphous (h_a)regions describe the morphology of the 1D-stack. Both are modeled by Gaussian distributions,

$$h_{a,c}(z) = \frac{1}{\sqrt{2\pi}\sigma_{a,c}} e^{-\frac{(z-d_{a,c})^2}{2\sigma_{a,c}^2}}. \tag{9}$$

Higher order distributions like for example the one for the long period h_{ac} are given by convolutions of the fundamental distributions $h_{a,c}$. By modeling $K''(z)$ or rather its cosine transform we can decompose it into the different contributions even if they overlap. To limit the effect of noise a window function $G(s) = e^{-4\pi^2 s^2 \sigma^2}$ is multiplied to the integrand in equation (7) before calculating the cosine transform. For all samples we used the same value $\sigma = 0.6$nm.

Rheology Linear viscoelastic properties of samples in the melt state were measured with a rheometer MCR501 from Anton Paar covering a frequency range from 628 rad/s to 0.1 rad/s and a temperature range from 90 to 50 °C. The samples were held between parallel plates with a diameter of 15 mm under nitrogen atmosphere. The sample thickness was 0.5 mm. The samples were prepared in a hot press at 85 °C for 10 min.

Differential scanning calorimetry Heat flow during isothermal crystallization and subsequent heating was recorded using a differential scanning calorimeter, UNIX DSC7 from Perkin Elmer. All samples were isothermally crystallized at 35 °C for 30 min after quenching from 85 °C. Finally all samples were heated to 85 °C again at a rate of 10 °C/min.

Mechanical Modulus The shear modulus of the samples in the semicrystalline state was measured with a rheometer Ares G2 from TA instruments at room temperature and a frequency of 10 rad/s in stripe geometry (sample length between clamps 25 mm, width 10 mm, thickness 1.2 mm). The samples were isothermally crystallized in a rectangular mold (Melt Prep) at 35 °C for 30 min.

Nuclear magnetic resonance (NMR) Measurements of the proton free induction decay (FID) were performed on a Bruker Avance III Spectrometer with a proton frequency of 200 MHz using a probe head with a short dead time of 2.5 µs. The time between successive scans was set to 3 to 5 s. The temperature accuracy of the instrument is ±1K with a gradient of

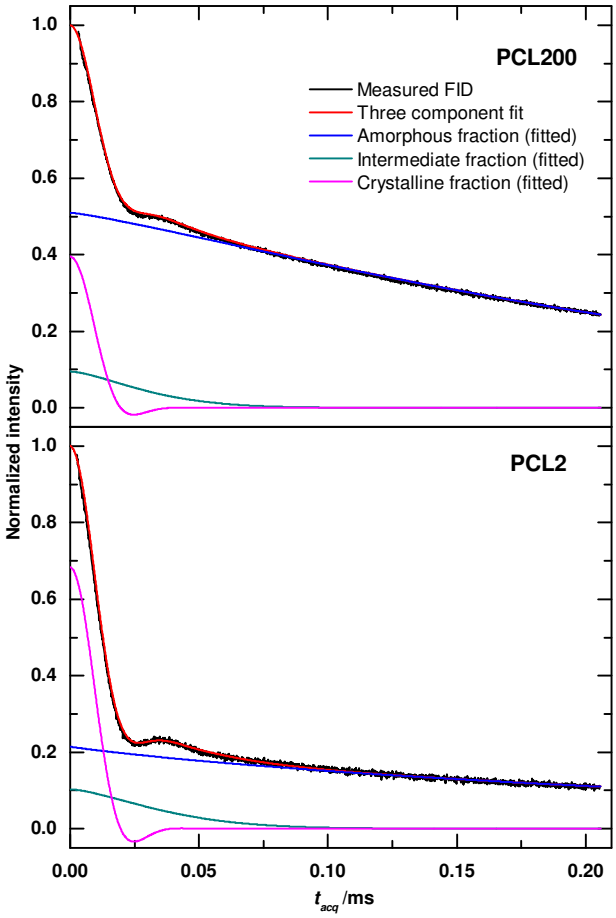

Figure 4: Measured FID and corresponding model fit based on a superposition of contributions from crystalline, amorphous and intermediate fractions for PCL200 (top) and PCL2 (bottom), cf. Eq. 10. FIDs were measured at 35°C on samples crystallized at 35°C.

0.5K over the sample. Samples for the analysis of the semicrystalline morphology were heated to 90 °C for 10 minutes to erase the thermal history and were then quenched to 35 °C for isothermal crystallization. After a crystallization time of several hours the measurements were performed at the crystallization temperature.

The different, partly motion-averaged dipole-dipole couplings in the crystalline, intermediate and amorphous regions allow a determination of the respective fractions by a three-component fit of the measured FIDs:

$$I_{FID}(t) = f_a \cdot e^{-(t/T^*_{2,a})^{\nu_a}} + f_i \cdot e^{-(t/T^*_{2,i})^{\nu_i}} + f_c \cdot e^{-(a^2t^2/2)} \cdot \frac{\sin(b \cdot t)}{b \cdot t} \tag{10}$$

The amorphous and intermediate components are fitted with stretched exponentials with apparent transverse relaxation times $T^*_{2,a}$ and $T^*_{2,i}$ and shape parameters ν_a, ν_i. Hereby the fit is stabilized by separate analysis of a MAPE-filtered FID, in which the signal from the crystalline and intermediate fractions are suppressed, resulting in a well-defined decomposition of the FID-signal into molar signal fractions of the amorphous, intermediate, and crystalline phases. Exemplary data are shown in Figure 4. Further details regarding the method and the analysis can be found in reference.[46]

References

(1) Flory, P. J.; Yoon, D. Y. Molecular morphology in semicrystalline polymers. Nature **1978**, 272, 226–229.

(2) Strobl, G. The physics of polymers. Concepts for understanding their structures and behavior, 3rd ed.; Springer: Berlin [u.a.], 2007; pp XIII, 518 S., DOI: 10.1007/978-3-540-68411-4.

(3) Men, Y.; Rieger, J.; Strobl, G. Role of the Entangled Amorphous Network in Tensile Deformation of Semicrystalline Polymers. Phys. Rev. Lett **2003**, 91, 095502–+.

(4) Bartczak, Z.; Kozanecki, M. Influence of molecular parameters on high-strain deformation of polyethylene in the plane-strain compression. Part I. Stress–strain behavior. Polymer **2005**, 46, 8210–8221, DOI: 10.1016/j.polymer.2005.06.100.

(5) Bartczak, Z. Deformation of semicrystalline polymers – the contribution of crystalline and amorphous phases. Polimery **2017**, 62, 787–799, DOI: 10.14314/polimery.2017.787.

(6) Hoffman, J. D.; Davis, G.; Lauritzen, J. I. In Treatise on Solid State Chemistry; Hannay, N., Ed.; Plenum Press: New York, 1976; Vol. 3; Chapter 7, pp 497–614.

(7) Sadler, D. M. New explanation for chain folding in polymers. Nature **1987**, 326, 174–177.

(8) Hu, W.; Frenkel, D.; Mathot, V. B. Intramolecular Nucleation Model for Polymer Crystallization. Macromolecules **2003**, 36, 8178–8183.

(9) Strobl, G. Crystallization and melting of bulk polymers: New observations, conclusions and a thermodynamic scheme. Progress in Polymer Science **2006**, 31, 398–442.

(10) Gedde, U. W. Polymer physics, 1st ed.; Chapman & Hall: London [u.a.], 1995; pp X, 298 S.

(11) Schulz, M.; Schäfer, M.; Saalwächter, K.; Thurn-Albrecht, T. Competition between crystal growth and intracrystalline chain diffusion determines the lamellar thickness in semicrystalline polymers. Nature Communications **2022**, 13, 119, DOI: 10.1038/s41467-021-27752-0.

(12) Iwata, K. Role of entanglement in crystalline polymers 1. Basic theory. Polymer **2002**, 43, 6609–6626.

(13) Mandelkern, L. The Structure of Crystalline Polymers. Accounts of Chemical Research **1990**, 23, 380–386, DOI: DOI ␣␣10.1021/ar00179a006.

(14) Psarski, M.; Piorkowska, E.; Galeski, A. Crystallization of polyethylene from melt with lowered chain entanglements. Macromolecules **2000**, 33, 916–932.

(15) Lippits, D.; Rastogi, S.; Talebi, S.; Bailly, C. Formation of entanglements in initially disentangled polymer melts. Macromolecules **2006**, 39, 8882–8885.

(16) Rastogi, S.; Lippits, D.; Peters, G.; Graf, R.; Yao, Y.; Spiess, H. Heterogeneity in polymer melts from melting of polymer crystals. Nature Materials **2005**, 4, 635–641.

(17) Lippits, D.; Rastogi, S.; Höhne, G.; Mezari, B.; Magusin, P. Heterogeneous distribution of entanglements in the polymer melt and its influence on crystallization. Macromolecules **2007**, 40, 1004–1010.

(18) Heck, B.; Strobl, G.; Grasruck, M. Characteristic variations in theeffect of diluents on polymer crystallization and meltingobserved for a sample of poly(ethylene-co-octene). The European Physical Journal E **2003**, 11, 117–130, DOI: 10.1140/epje/i2002-10151-8.

(19) Tian, N.; Liu, D.; Wei, H. H.; Liu, Y. P.; Kong, J. Crystallization of polycaprolactone with reduced entanglement. European Polymer Journal **2018**, 102, 38–44, DOI: 10.1016/j.eurpolymj.2018.03.017.

(20) Rubinstein, M. Polymer Physics; Oxford University Preess, Inc.: United States, 2003.

(21) Luo, C.; Sommer, J. Role of Thermal History and Entanglement Related Thickness Selection in Polymer Crystallization. ACS Macro Lett **2016**, 5, 30–34, DOI: 10.1021/acsmacrolett.5b00668.

(22) Luo, C.; Kröger, M.; Sommer, J. Entanglements and Crystallization of Concentrated Polymer Solutions: Molecular Dynamics Simulations. Macromolecules **2016**, 49, 9017–9025.

(23) Kurz, R.; Schulz, M.; Scheliga, F.; Men, Y.; Seidlitz, A.; Thurn-Albrecht, T.; Saalwächter, K. Interplay between Crystallization and Entanglements in the Amorphous Phase of the Crystal-Fixed Polymer Poly(ε-caprolactone). Macromolecules **2018**, 51, 5831–5841, DOI: 10.1021/acs.macromol.8b00809.

(24) Ferry, J. Viscoelastic Properties of Polymers; 1980.

(25) Booij, H.; Thoone, G. Generalization of Kramers-Kronig transforms and some approximations of relations between viscoelastic quantities. Rheol. Acta **1982**, 21, 15–24.

(26) Liu, K.; de Boer, E.; Yao, Y.; Romano, D.; Ronca, S.; Rastogi, S. Heterogeneous Distribution of Entanglements in a Nonequilibrium Polymer Melt of UHMWPE: Influence on Crystallization without and with Graphene Oxide. Macromolecules **2016**, 49, 7497–7509.

(27) Wu, S. Dynamic rheology and molecular weight distribution of insoluble polymers: tetrafluoroethylene-hexafluoropropylene copolymers. Macromolecules **1985**, 18, 2023–2030.

(28) Liu, C.; He, J.; van Ruymbeke, E.; Keunings, R.; Bailly, C. Evaluation of different methods for the determination of the plateau modulus and the entanglement molecular weight. Polymer **2006**, 47, 4461–4479.

(29) Colby, R. H.; Rubinstein, M. Two-parameter scaling for polymers in Θ solvents. Macromolecules **1990**, 23, 2753–2757, DOI: 10.1021/ma00212a028.

(30) Mark, J. E. Physical Properties of Polymers Handbook; Springer: New York, 2007; pp I–XX; 1–1076, DOI: 10.1007/978-0-387-69002-5.

(31) Seidlitz, A.; Thurn-Albrecht, T. In Polymer Morphology; Guo, Q., Ed.; 2016; pp 151–164, DOI: 10.1002/9781118892756.ch9.

(32) Schulz, M.; Seidlitz, A.; Kurz, R.; Barenwald, R.; Petzold, A.; Saalwachter, K.; Thurn-Albrecht, T. The Underestimated Effect of Intracrystalline Chain Dynamics on the Morphology and Stability of Semicrystalline Polymers. Macromolecules **2018**, 51, 8377–8385, DOI: 10.1021/acs.macromol.8b01102.

(33) Schulz, M.; Seidlitz, A.; Petzold, A.; Thurn-Albrecht, T. The effect of intracrystalline chain dynamics on melting and reorganization during heating in semicrystalline polymers. Polymer **2020**, 196, 122441, DOI: 10.1016/j.polymer.2020.122441.

(34) Kurz, R.; Achilles, A.; Chen, W.; Schäfer, M.; Seidlitz, A.; Golitsyn, Y.; Kressler, J.; Paul, W.; Hempel, G.; Miyoshi, T.; Thurn-Albrecht, T.; Saalwächter, K. Intracrystalline Jump Motion in Poly(ethylene oxide) Lamellae of Variable Thickness: A Comparison of NMR Methods. Macromolecules **2017**, 50, 3890–3902.

(35) Ungar, G.; Zeng, K. Learning polymer crystallization with the aid of linear, branched and cyclic model compounds. Chemical Reviews **2001**, 101, 4157–4188.

(36) Takizawa, K.; Tang, C.; Hawker, C. J. Molecularly Defined Caprolactone Oligomers and Polymers: Synthesis and Characterization. Journal of the American Chemical Society **2008**, 130, 1718–1726, DOI: 10.1021/ja077149w.

(37) Fritzsching, K.; Mao, K.; Schmidt-Rohr, K. Avoidance of Density Anomalies as a Structural Principle for Semicrystalline Polymers: The Importance of Chain Ends and Chain Tilt. Macromolecules **2017**, 50, 1521–1540.

(38) Cho, T.; Stille, W.; Strobl, G. Zero growth temperature and growth kinetics of crystallizing poly(epsilon-caprolactone). Colloid and Polymer Science **2007**, 285, 931–934.

(39) Luo, C.; Sommer, J. Frozen Topology: Entanglements Control Nucleation and Crystallization in Polymers. Physical Review Letters **2014**, 112, 195702–+.

(40) Jin, F.; Yuan, S.; Wang, S.; Zhang, Y.; Zheng, Y.; Hong, Y.-l.; Miyoshi, T. Polymer Chains Fold Prior to Crystallization. ACS Macro Letters **2022**, 11, 284–288.

(41) Wunderlich, B.; Arakawa, T. Polyethylene crystallized from the melt under elevated pressure. Journal of Polymer Science Part A: General Papers **1964**, 2, 3697–3706, DOI: https://doi.org/10.1002/pol.1964.100020828.

(42) Hu, H.; Dorset, D. Crystal-Structure of Poly(e-Caprolactone). Macromolecules **1990**, 23, 4604–4607.

(43) Huang, Y.; Xu, Z. D.; Huang, Y. P.; Ma, D. Z.; Yang, J. C.; Mays, J. W. Characterization of poly(epsilon-caprolactone) via size exclusion chromatography with online right-angle laser-light scattering and viscometric detectors. International Journal of Polymer Analysis and Characterization **2003**, 8, 383–394, DOI: 10.1080/714975019.

(44) Ruland, W. The evaluation of the small-angle scattering of lamellar two-phase systems by means of interface distribution functions. Colloid & Polymer Sci **1977**, 255, 417–427.

(45) Qiao, Y.; Schulz, M.; Wang, H.; Chen, R.; Schäfer, M.; Thurn-Albrecht, T.; Men, Y. Hierarchical structure of polybutene-1 in crystal blocks resulting from the form II to I solid-to-solid transition as revealed by small-angle X-ray scattering. Polymer **2020**, 195, 122425, DOI: 10.1016/j.polymer.2020.122425.

(46) Schäler, K.; Roos, M.; Micke, P.; Golitsyn, Y.; Seidlitz, A.; Thurn-Albrecht, T.; Schneider, H.; Hempel, G.; Saalwächter, K. Basic principles of static proton low-resolution spin diffusion NMR in nanophase-separated materials with mobility contrast. Solid State Nuclear Magnetic Resonance **2015**, 72, 50–63.

Acknowledgement We thank Kathrin Herfurt for technical help with DSC measurements and Jonas Warneke for crosschecking the MW of the oligomer material by mass spectrocopy. Funding was provided by the Ministry of Science, Energy, Climate Protection and

Environment of the State of Saxony-Anhalt (grant no. 41-04032/2018) (ZW, TTA) and the Deutsche Forschungsgemeinschaft (DFG, German Research Foundation) – Project-ID 189853844 – TRR 102 (K.S. and T.T.-A.).

Correspondence Correspondence and requests for materials should be addressed to T. T.-A. (thurn-albrecht@physik.uni-halle.de)

Supplementary Information Supplementary Information is available.

- Figure S1: Original rheology data
- Figure S2: Determination of the plateau modulus of Polycaprolactone
- Supplementary Text 1: Entanglement threshold
- Figure S3: Full DSC data
- Supplementary Text 2: : Quantitative analysis of the SAXS data
- Figure S4: Background subtraction SAXS data
- Figure S5: Determination of Porod constant and contribution from density fluctuations
- Figure S6: Interface distribution function in reciprocal space
- Figure S7: Interface distribution function in real space
- Figure S8: Assignment of structural parameters from SAXS-heating experiments
- Figure S9: Comparison of the decomposition of the amorphous fraction by SAXS and NMR
- Figure S10: Mechanical properties of the polymer/oligomer blends in the solid state

Supplementary Files

This is a list of supplementary files associated with this preprint. Click to download.

- SupplementaryInformationv12dtta.pdf